RESEARCH PAPER

Synthesis of iron nanoparticles in poly(N-isopropylacrylamide-acrylic acid) hybrid microgels for catalytic reduction of series of organic pollutants: a first approach

Shanza Rauf Khan [iD] · **Sarmed Ali** · **Burhan Ullah** · **Saba Jamil** · **Tanzeela Zanib**

Abstract First approach towards in situ synthesis of iron (Fe) nanoparticles within poly(N-isopropylacrylamide-acrylic acid) (p(NIPAM-AA)) microgel is established in this work. Morphology, size, and size distribution of Fe-p(NIPAM-AA) hybrid microgel are confirmed by FTIR, STEM, and UV-Vis spectroscopy. Size of majority of Fe nanoparticles lies in 5–25-nm range, and very few nanoparticles lie in 30–40-nm range. Reduction of series of substrates with similar and dissimilar chemical structure is catalyzed by synthesized Fe-p(NIPAM-AA) hybrid microgel. Catalytic activity of hybrid microgel towards various substrates is studied by comparing their apparent rate constant (k_{app}), reduction time, and percentage reduction. Catalytic activity of hybrid microgel towards reduction of nitroarenes is observed higher than that of azo dyes. Repulsion among carboxyl groups (COOH) of AA facilitated the flux of substrates inside the microgel network. Significant difference among k_{app}, reduction time, and percentage reduction of all substrates is observed. k_{app} of crystal violet is observed maximum among all substrates. Percentage conversion of 4-nitroanisole is observed highest among all substrates. Similar values of k_{app}, reduction time, and reduction percentage of all nitrophenols are obtained, while significant difference in values of k_{app}, reduction time, and reduction percentage of all azo dyes is observed. Catalytic reduction of all substrates is compared on the basis of orientation of functional groups, presence of bulky groups, and number of bonds to be reduced.

Introduction

Nitroarenes and organic azo dyes are organic pollutants and originated from food (Yamjala et al. 2016), paper (Calace et al. 2002) and dying industrial effluents (Sarkar et al. 2017) and domestic runoff (Ott and Roberts 1998). Physiochemical (flocculation, coagulation, filtration, and adsorption) (Wang and Chen 2015), ultraviolet radiation (Pawar et al. 2014), and chemical oxidation (Martinez-Huitle and Ferro 2006) methods are used to reduce the organic pollutants. Nanotechnology is a promising technique and developing very fast in the present decade. High surface area to volume ratio of nanoparticles shows tremendous capability in the field of sensing (Zhang et al. 2011), catalysis (Hudson et al. 2013), drug delivery (Ulbrich et al. 2016), and adsorption (Abid et al. 2013). Organic pollutants are reduced

S. R. Khan (✉) · B. Ullah · S. Jamil · T. Zanib
Department of Chemistry, University of Agriculture,
Faisalabad 38000, Pakistan
e-mail: shanzaraufkhan@gmail.com

S. Ali
Department of Physics, University of Agriculture,
Faisalabad 38000, Pakistan

S. Jamil
Department of Materials Science and Engineering, Cornell
University, Ithaca 14853, USA

using nanoparticles as catalyst (Bhattacharjee et al. 2015; Dong et al. 2014; Edison and Sethuraman 2013; Ghosh et al. 2015; Veerakumar et al. 2015). Adhesive forces among nanoparticles accumulate them. Stabilization of nanoparticles for long time is a challenging task for researchers. Micelles (Yoo et al. 2007), polysaccharides (Chang et al. 2011), dendrimers (Shi et al. 2008), and microgels (Biffis et al. 2007) are used as stabilizing agents to overcome the accumulation of nanoparticles. Owing to crosslinked structure, microgels creates physical barrier against free movement of nanoparticles. Smart polymeric microgels are responsive to external stimuli like pH (Wu et al. 2012), temperature (Liu et al. 2012), and ionic strength (Karg et al. 2008). So, multiresponsive microgels show on/off characteristics for controlling the catalytic activity of nanoparticles (Bhattacharya et al. 2007; Pich et al. 2006a, b). In situ synthesis of copper (Shahid et al. 2019), gold (Wunder et al. 2011), silver (Farooqi et al. 2015a, b), platinum (Naseem et al. 2018), and palladium (Chen et al. 2019) nanoparticles within microgels for catalytic reduction of nitroarenes have been reported. In situ synthesis of iron (Fe) nanoparticles has not been reported previously. Effect of various parameters on apparent rate constant (k_{app}) of catalysis has been reported. Dependence of k_{app} on catalyst dosage (Farooqi et al. 2015a, b) and composition of microgel have been studied (Farooqi et al. 2014). Change in kinetics of 4-nitrophenol (4-NP) reduction by increasing gold nanoparticles dose and temperature have been studied (Pich et al. 2006a, b). Various nitroarenes have been catalytically reduced by using hybrid microgels. For example, catalytic reduction of methylene blue (MB) and Congo red (CR) dyes using silver and gold nanoparticles fabricated poly(N-isopropylacrylamide-methacrylic acid-2-hydroxyethyl methacrylate) microgels have been studied (Shah et al. 2016). Comparison of catalytic reduction of nitrophenols (Soğukömeroğulları et al. 2019) and organic azo dyes has been reported (Pouretedal and Sabzevari 2011). Reduction of series of pollutants of different structures and positions and orientations of reducible functional groups using single catalyst is a subject of interest for the scientists. This works diverts attention of scientists towards synthesis of such catalytic devices which have capacity to reduce range of substrates. Previously, reasoning involved in catalytic reduction of nitroarenes and azo dyes have not been explained. In this work, role of different factors, i.e., orientation of nitro groups, presence of bulky groups

and number of targeted bonds to be reduced in increasing/decreasing the k_{app} of catalytic reduction of substrates is comprehensively discussed. Herein, catalytic activity of Fe-p(NIPAM-AA) microgel is studied for reduction of nitrophenols and organic azo dyes. The dependence of reduction of nitroarenes and azo dyes on their structure is studied in this work. Significant difference in k_{app} of nitroarenes and azo dyes is observed. First approach is also developed for synthesis of p(NIPAM-AA) microgel loaded with Fe nanoparticles. Composition of microgel and size of Fe nanoparticles is characterized by FTIR, STEM, and UV-Vis spectroscopy.

Materials and methods

Materials

All reagents acrylic acid (AA), ammonium per sulfate (APS), N,N-methylene bisacrylamide (BIS), Congo red dye (CR), crystal violet (CV), 2,4-dinitrophenol (DNP), ferric chloride hexahydrate ($FeCl_3 \cdot 6H_2O$), methyl blue (MB), methyl red (MR), N-isopropylacrylamide (NIPAM), 4-nitrophenol (4-NP), 3-nitrophenol (3-NP), 4-nitrobenzoic acid (4-NBA), 4-nitroanisole (4-NAS), reactive black 5 (RB5), and sodium dodecyl sulfate (SDS) were purchased from Sigma-Aldrich, USA. All the chemicals except AA are used as such, without any further purification. AA was purified by using aluminum oxide (Al_2O_3) via filtration under reduced pressure to remove hydroquinone inhibitor.

Synthesis of p(NIPAM-AA) microgel

p(NIPAM-AA) microgel was synthesized by free radical emulsion polymerization. NIPAM (0.92 g) (0.8 mmol), 0.4 mL AA (0.7 mmol), 0.07 g BIS, and 0.05 g of SDS were dissolved in 95 mL distilled water in a 250-mL three-neck round-bottom flask. Resultant solution was purged with nitrogen gas and stirred for 30 min at 70 °C. Five milliliters of APS (0.05 mM) was dropwise added into resultant solution and stirred for 4 h at 70 °C. Later microgel sample was cooled to room temperature. Synthesized p(NIPAM-AA) microgel was dialyzed against distilled water for 1 week using molecular porous membrane tubing MW 12,000–14,000.

In situ synthesis of Fe nanoparticles within p(NIPAM-AA) microgel

Fe nanoparticles were synthesized within p(NIPAM-AA) microgel network using in situ reduction. Synthesized p(NIPAM-AA) microgel was used as template for the synthesis of Fe-p(NIPAM-AA) hybrid microgel. Ten milliliters p(NIPAM-AA) microgel dispersion and 7 mL water were added into round-bottom flask and stirred for 30 min at pH 9. Now 0.9 mL of $FeCl_3 \cdot 6H_2O$ (0.01 M) was added into microgel dispersion and stirred for 30 min at 25 °C. Then, 0.01 g $NaBH_4$ was added and stirred for another 60 min. Then, hybrid microgel was dialyzed against distilled water using semipermeable membrane.

Catalytic application of Fe-p(NIPAM-AA) hybrid microgel

Fe-p(NIPAM-AA) hybrid microgel was used as catalyst for reduction of 3-NP, 4-NP, DNP, 4-NAS, 4-NBA, CR, CV, MB, MR, and RB5. Catalytic role of hybrid microgel was studied using UV-Vis spectroscopy. Substrate solution (3.5 mL) (0.1 mM), $NaBH_4$ (0.01 mg), and 0.5 mL hybrid microgel dispersion were taken into cuvette. Spectra were scanned until change in absorbance was not observed at λ_{max} of substrate and color of solution was changed to colorless. The absorbance of substrate solution at 0 min is noted as A_0. The absorbance of substrate solution at any time t is noted as A_t. Value of apparent rate constant (k_{app}) is determined from Eq. (1).

$$\ln\left(\frac{A_t}{A_0}\right) = -k_{app} \times t \qquad (1)$$

Characterization

BMS Vis 1100 spectrophotometer available at Post Agriculture Research Station, Community College, University of Agriculture Fasialabad was used for UV-Vis spectroscopic analysis of Fe-p(NIPAM-AA) hybrid microgel. Nanoparticle size was measured using STEM. FEI NOVE 450 NANOSEM with EDX available at Syed Babar Ali School of Science and Engenerieng, Lahore University of Management and Sciences, Lahore, Pakistan, is used to obtain STEM image of hybrid microgel. Perkin Elmer FTIR spectrophotometer available at Punjab Bio-Energy Institute, University of Agriculture, Faiasalabad, is used for functional group analysis of Fe-p(NIPAM-AA) hybrid microgel. Size distribution of microgel particles is obtained from dynamic light scattering (DLS) BI-200SM (Brookhaven Instruments Corporation) at 90° scattering angle with 632.8 nm helium-neon laser light source.

Results and discussion

Synthesis of p(NIPAM-AA) microgel

p(NIPAM-AA) microgel is synthesized by free radical emulsion polymerization. NIPAM is insoluble at $T >$ 32 °C. APS is dissociated into persulfate ions ($S_2O_8^{2-}$) at 70 °C and decomposed into anionic sulfate radicals S_4^{2-} in initiation reaction. Decomposition of S_4^{2-} is increased with increase in temperature. S_4^{2-} was reacted with AA and NIPAM and polymerization was initiated. S_4^{2-} radicals are attached at one end of polymeric chain while other end of polymeric chain is negatively charged. Polymeric chains are grown to a certain critical length to form precursor particles during propagation. Macrogelation of p(NIPAM-AA) is restricted due to repulsion between negatively charged end of p(NIPAM-AA) chains. Anionic part of polymer provides stability to growing chains. Size of precursor is increased after the crosslinking among polymeric chains. BIS crosslinker is stabilized dense polymeric network of p(NIPAM-AA) gel and increased its mechanical strength. SDS layer is present around microgel particles which hindered their agglomeration. So, adsorption of SDS around particles stabilizes microgel network.
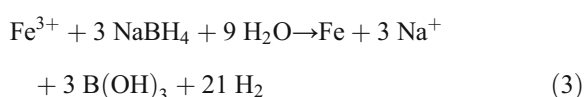
In situ synthesis of Fe nanoparticles within p(NIPAM-AA) microgel

The complete mechanism of in situ synthesis of Fe nanoparticles within p(NIPAM-AA) microgel is shown as Fig. 1. Fe nanoparticles are synthesized at pH 9 of medium. Carboxyl groups (COOH) of functional monomer AA are homogenously distributed within the whole network of microgel which is ionized into carboxylate ions (COO^-) at pH 9. Microgel gates are opened due to repulsive interactions among these COO^-. Ionization of $FeCl_3 \cdot 6H_2O$ is taken place at pH 9, and ionized Fe^{3+} is fluxed through these opened microgel gates.

Fig. 1 Free radical emulsion synthesis of p(NIPAM-AA) microgels and in situ synthesis of Fe nanoparticles within p(NIPAM-AA) microgels
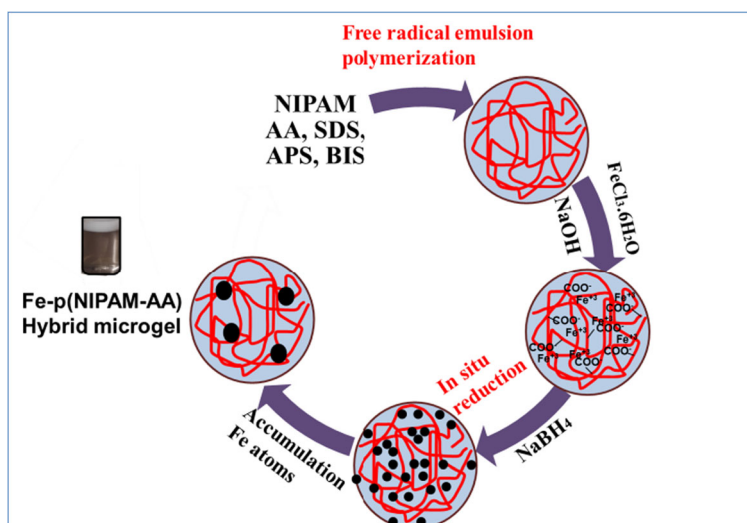
Electrostatic attractive interactions are established between Fe^{3+} and COO^-, and Fe^{3+} was successfully incorporated into the whole microgel network. $NaBH_4$ was reduced the Fe^{3+} into Fe^0 atoms (Eqs. 2–4). Adhesive forces among Fe atoms accumulate them and grown up to certain size. Growth of Fe atoms depends on sieves size of microgel network. Carboxyl groups of AA are served as center to capture Fe nanoparticles. Dense polymeric microgel network is acted as physical barrier against movement of Fe nanoparticles. So Fe nanoparticles do not grow into macroparticles.

$$FeCl_3 \cdot 6H_2O \leftrightarrow Fe^{3+} + 3\,Cl^- + 6\,H_2O \qquad (2)$$

$$Fe^{3+} + 3\,NaBH_4 + 9\,H_2O \rightarrow Fe + 3\,Na^+$$
$$+ 3\,B(OH)_3 + 21\,H_2 \qquad (3)$$

$$3\,Na^+ + 3\,Cl^- \rightarrow 3\,NaCl \qquad (4)$$

Characterization of hybrid microgel

STEM and DLS

Figure 2 a shows the STEM image of synthesized hybrid mirogel. Fe nanoparticles are sucessfully synthesized within microgel network. Size of microgel particles lies in 300–1200-nm range. Dark spots in Fig. 2a are indicated the presence of Fe nanoparticles. Different size of dark spots shown in Fig. 2a confirmed that size of Fe nanoparticles within microgel network is not same. Few nanoparticles are of big size while most of the nanoparticles are of small size. Fe nanoparticles are indicated by red circles with in single microgel particle. Size of Fe nanoparticles lies in 5–40-nm range. Size distribution histogram of Fe nanoparticles and microgels are given as Fig. 2 b and c, respectively. Figure 2 b shows that size of majority of particles lies in 5–25-nm range while size of few particles lies in 30–40-nm range. Figure 2 c shows that size of majority of particles lies in 400–1000-nm range. It is observed from STEM images that nanoparticles are 1–6 nm apart from each other. Size of nanoparticles depends on size microgel sieve. Size of gel lies in micro range, so the sieve size lies in nano range.

UV-Vis spectroscopy

Two SPR bands are observed in Fig. 2d obtained after UV-Vis spectroscopic analysis. UV-Vis spectra of NIPAM, BIS, and AA is shown in Fig. 2e. NIPAM, AA, and BIS are transparent to UV-Vis range. Therefore, no obsorbace peaks are observed in their UV-Vis spectra. Dipolar oscillations of nanoparticles resonate with incoming light at specific frequency which is dependent on particle sizes (Huang and El-Sayed 2010). Surface plasmon resonance (SPR) band is observed at shorter wavelength due to small size nanoparticles, while SPR band found at longer wavelength indicated the presence of bigger size nanoparticles. Extinction of SPR bands in UV-Vis spectra indicating different size
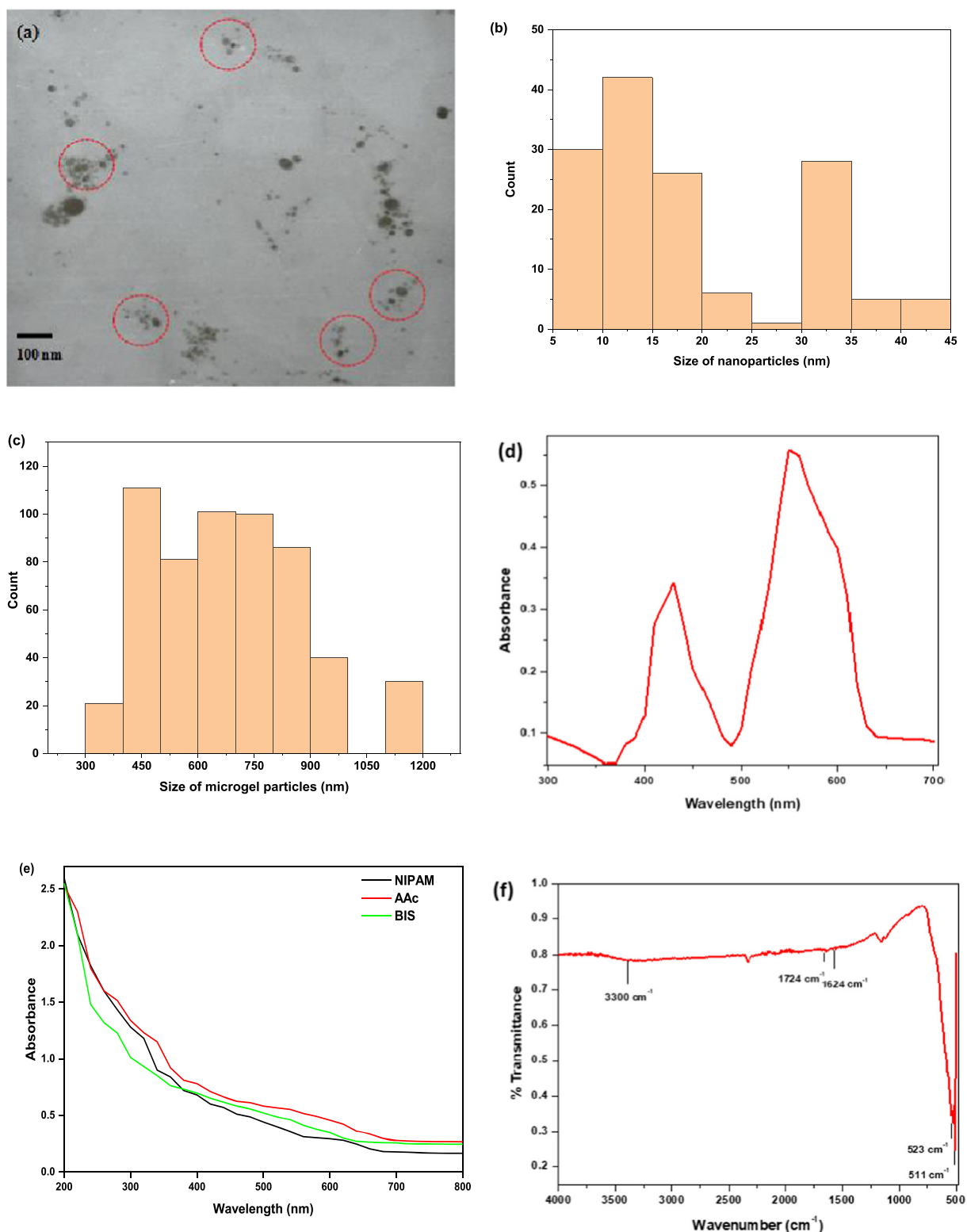
Fig. 2 Charatcerization of Fe-p(NIPAM-AA) hybrid microgel: **a** STEM; **b**, **c** size distribution histogram of Fe nanoparticles and microgel particles; **d** UV-Vis spectroscopy; **e** UV-Vis spectra of NIPAM, BIS, and AA; and **f** FTIR

distribution of gold nanoparticles has been reported (Huang and El-Sayed 2010). Presence of two SPR bands in UV-Vis spectra indicated the different size distribution of Fe nanoparticles inside p(NIPAM-AA) microgel network. SPR band at wavelength 590 nm is due to big nanoparticles while SPR band at wavelength 445 nm is due to small nanoparticles. Polydispersity of bigger size Fe nanoparticles are shown by the presence of broad band around 590 nm. Presence of different SPR bands belong to different sizes of Fe nanoparticles (Eslami et al. 2018). Polydisperesity of Fe nanoparticles within whole network of p(NIPAM-AA) microgel is also confirmed by study of STEM image as shown in Fig. 2a.

FTIR

FTIR pattern of Fe-p(NIPAM-AA) hybrid microgel is shown as Fig. 2f. FTIR spectrocopy is used to study the functional group analysis of synthsized Fe-p(NIPAM-AA) hybrid microgel. Presence of unreacted elements and formtion of microgel is confimed by the analysis of absorption peaks of FTIR spectra shown in Fig. 2f. Presence of absorption band around 1664 cm^{-1} confirmed the presence of AA within Fe-p(NIPAM-AA) microgel network. Presence of absorption band around 1724 cm^{-1} of C=O confirmed the presence of NIPAM within Fe-p(NIPAM-AA) microgel network. Hydroxyl (–OH) functional group absorbs around 3300 cm^{-1} and gives broad band. Appearance of broad band around 3300 cm^{-1} of –OH indicated the presence of water molecules inside the microgel network. Absence of absoption band around the 1550–1600 cm^{-1} of C=C in the FTIR spectra is confirmed that no unreacted NIPAM and AA is persent within microgel network. Presence of peaks around 400–750 cm^{-1} indicates the presence of Fe nanoparticles (Khan et al. 2016; Velayudhan Nair Girija and Vasu 2019). FTIR spectra shows two peaks around 511 and 523 cm^{-1} which confirm Fe-Fe coordination. So, FTIR analysis confirms the synthesis of Fe-p(NIPAM-AA) hybrid microgel. However, FTIR spectra of NIPAM have been reported previously (Khan et al. 2016). All the peaks of NIPAM can be clearly observed around 400–750 cm^{-1}. FTIR spectra of poly(N-isopropylacrylamide-allylacetic acid) and silver-poly(N-isopropylacrylamide-allylacetic acid) are also compared. It is observed previously that NIPAM and silver-silver (Ag-Ag) bonds absorbed in 400–750 cm^{-1} region. So peaks in this region have broadened.

Therefore, it is claimed in this manuscript that FTIR peaks related to metal-metal bond are also observed in this region (400–750 cm^{-1}).

Study of catalytic reduction of substrates

Catlytic reduction and k_{app} of series of substrates were studied using synthesized hybrid microgel as catalyst. Nitroarenes and azo dyes were reduced into its amino derivatives using $NaBH_4$ as reducing agent and Fe nanoparticles as catalyst. Catalytic reduction of substrates depends on time as shown in Fig. 3a, b. Significant reduction of substrates was observed by linear region of plot. Microgel gates were opened due to repulsion among COO^-, and borohydride ions (BH_4^-) and substrates are passsed through these gates. Extent of catalytic reduction of substrates depends on flux of reactants, availability of reactants, free active sites, and hindrance due to bulky groups around the azo bond. Size distribution histogram of nanoparticles is given in Fig. 2b. Histogram shows that particles of two different sizes have synthesized. Therefore, two different average sizes are discussed under subsection "STEM and DLS." Microgels acts as stabilizers and prevents the aggregation of nanoparticles. But very small nanoparticles diffuse and coalesce with other nanoparticles and formed big nanoparticles. Therefore, few nanoparticles are of big size. Efficiency of catalyst depends on surface to volume ratio as size of nanoparticles is decreased then active surfaces are increased. But catalytic reduction variates due to presence of different average sizes of particles. Small nanoparticles shown faster reduction of substrates as compared to that of big nanoparticles. So catalytic efficiency of hybrid microgel is lowered due to presence of polydispersity of nanoparticles. Catalytic reduction of substrates obeys pseudo-first-order kinetics because $NaBH_4$ is used in excess. Catalytic reduction of 4-NAS is faster than other similar nitrophenols: 4-NP, 3-NP, DNP, and 4-NBA (Fig. 3a). Molecules of 4-NAS are of small size and rapidly adsorbed on the active sites of Fe nanoparticles. Bulky groups are not oriented around nitro group in 4-NAS, due to which its nitro group is easily reduced. Chemical structure of 4-NAS shows some similarity with 4-NP, so molecules of 4-NAS and 4-NP shows comparable values of k_{app} as compared to other members of nitrophenols series. Figure 3 b shows reduction of CV and RB5 is faster than CR, MB, and MR. Fast reduction of CV is due to minimum hindrance by bulky groups. Azo bond of
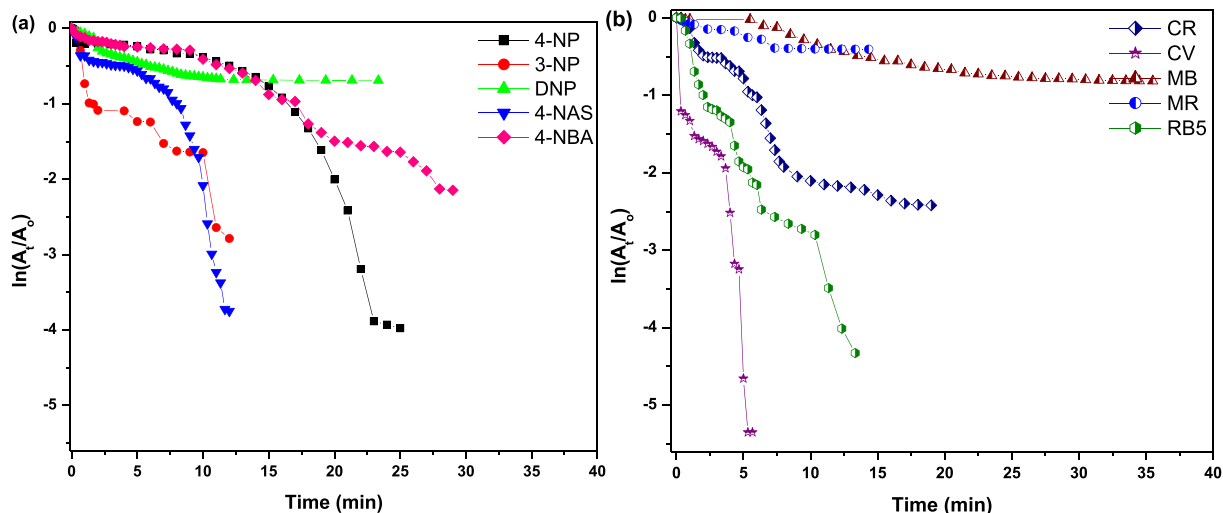
Fig. 3 Plot between ln (A_t/A_o) and time of catalytic reduction of **a** nitroarenes and **b** azo dyes (conditions: 3.5 mL substrate (0.1 mM), 0.01 mg NaBH$_4$, and 0.5 mL catalyst dispersion)
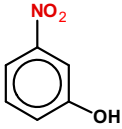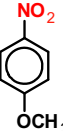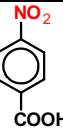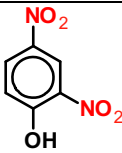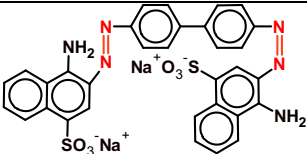
CV is present apparently at end of structure and shows minimum hindrance of bulky groups. Therefore, transfer of electron density is more easy in CV as compared to other dyes. More bulky groups are present around azo bond in RB5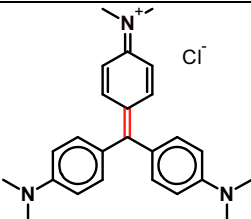 as compared to other azo dyes. Two azo bonds are present in RB5. More number of azo bonds in RB5 structure are responsibe for the faster reduction of RB5 than CR, MB, and MR. Reaction of azo bond with BH$_4^-$ is hindered due to more bulky groups around the azo bond in MR as compared to other respective azo dyes CV, CR, MB, and RB5. The catalytic reduction of MR is slowest than that of all other substrates as shown in Fig. 3a. Presence of bulky aromatic rings in MR was hindered the attack of BH$_4^-$ on azo bond. So azo bond of MR was not easily reduced as compared to all other substrates (Table 1).

Study of comparison of k$_{app}$ values

Figure 4 a shows the plot of k$_{app}$ of all substrates reduced using hybrid microgel as catalyst. The decerasing trend of k$_{app}$ of substares is as follows: CV > RB5 > 4-NAS > 3-NP > CR > 4-NP > 4-NBA > DNP > MR > MB. k$_{app}$ values of CV, RB5, 4-NAS, 3-NP, CV, 4-NP, 4-NBA, DNP, MR, and MB are observed as 0.749, 0.298, 0.252, 0.175, 0.145, 0.135, 0.070, 0.031, 0.030, and 0.026 min^{-1}, respectively. BH$_4^-$ attacks azo bond and nitro groups of substrates. The reduction of CV and RB5 is fastest among all substrates. k$_{app}$ value of CV is found highest among all substrates. Presence of CV and RB5 is found highest among all substrates. Presence of

open oriented azo bonds and less bulky groups around azo bonds in CV and RB5 is facilitated the fast reduction of azo bonds. Positively charged nitrogen atom of CV is highly electrophilic and favored the nucleophilic attack of BH$_4^-$. RB5 has oriented azo bonds and less number of bulky groups among all substrates. RB5 possess two nitro groups with no hindrance of bulky groups, so probability of electron density transfer is higher in RB5 than 4-NAS. Therefore, reduction of RB5 was faster than 4-NAS. Comparison of k$_{app}$ values shows that reduction of nitrophenols is faster as compared to azo dyes. Catalytic reduction of 4-NAS is slightly higher among the series of nitrophenols as shown in Fig. 4a. 4-NAS is rapidly adsorbed on active sites of Fe nanoparticles as compared to nitrophenols. Catalytic reduction of 4-NAS was observed greater than other nitrophenols due to rapid electron density transfer and high contact time with Fe nanoparticles. Figure 4 a shows that k$_{app}$ value of MR and MB are smallest among all substrates. The mobility of MB and MR through microgel sieves is lowered due to dissimilarity between microgel sieve and complex structure of MB and MR. The transfer of electron density has faced maximum hindrance due to presence of azo bonds inside the bulky groups. Therefore, MB and MR are not easily reduced. Shah et al. have studied the decreasing trend of k$_{app}$ of organic pollutants as MB > 4-NP > CR using poly (N-isopropylacrylamide–methacrylic acid-2-hydroxy methacrylate) loaded with silver and gold nanoparticles as catalyst (Shah et al. 2016). Fu et al. have been
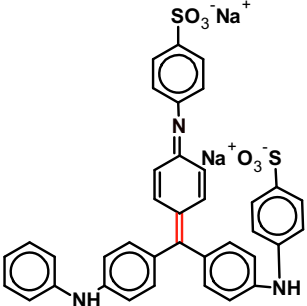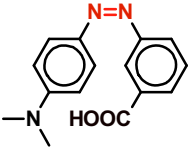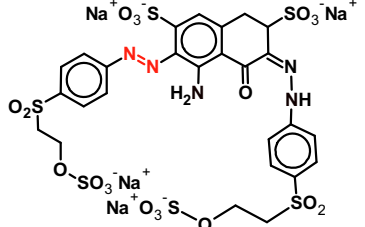
Table 1 Summary of initial, final, reduced concentrations of dyes along with figures of sample before and after reduction

Substrate		Initial concent ration (mM)	Final concentration (mM)	Reduced concentration (mM)	Intrinsic rate constant (mL/min µg)	Apparent half life (min)
3-NP		0.875	0.021	0.854	0.263	3.960
4-NP		0.875	0.0109	0.8641	0.203	5.133
4-NAS		0.875	0.010	0.8641	0.378	2.750
4-NBA		0.875	0.209	0.666	0.105	9.900
DNP		0.875	0.189	0.686	0.046	22.35
CR		0.875	0.105	0.770	0.218	4.779
CV		0.875	0.028	0.847	1.125	0.925

observed k_{app} trend of nitrophenols and azo dyes of 4-NP > DNP > CR is 0.00319 > 0.00203 > 0.00115 min^{-1} using gold nanoparticles decorated on activated coke (Fu et al. 2019). Significant difference in k_{app} values of azo dyes is observed due to dissimilarity in their structure while k_{app} values of series nitroarenes are similar which differs only in position of nitro group.

Table 1 (continued)

	Structure					
MB	(chemical structure)	0.875	0.139	0.736	0.039	26.65
MR	(chemical structure)	0.875	0.333	0.542	0.045	23.10
RB5	(chemical structure)	0.875	0.0109	0.856	0.447	2.325

Comparison of percentage reduction

Figure 4 b shows the plot of comparison of percentage reduction of substrates using synthesized hybrid microgel as catalyst. Figure 4 b shows the decreasing trend of percentage reduction as 4-NAS > 4-NP > RB5 > 3-NP > CV > CR > MB > DNP > 4-NBA > MR. Values of percentage reduction of 4-NAS, 4-NP, RB5, 3-NP, CV, CR, MB, DNP, 4-NBA, and MR are observed as 98.7, 98.3, 97.9, 97.6, 96.8, 88.1, 84.1, 78.4, 76.1, and 61.9% respectively. Figure 4 b shows that percentage reduction of 4-NAS, 4-NP, and RB5 are almost equal to each other. Percentage reduction of 4-NAS is found highest among the series of substrates. The flux of 4-NAS is high due to its small size because diffusion of small molecules is greater than big molecules. Number of adsorbed 4-NAS molecules is greater than that of big molecules. Availability of active surfaces was increased the adsorption of BH_4^- and 4-NAS. Molecules of 4-NAS and 4-NP are shown structural similarity, so percentage conversion of 4-NAS and 4-NP are same. Complex structure of RB5 azo dyes was decreased its flux and adsorption. Minimum hindrance of bulky groups is facilitated the electron density tranformation. Trend of percentage reduction shows the minimum percentage reduction in MR as compared to other substrates. Bulky groups are present around azo bond in MR which hindered the transfer of electron density. The percentage reduction of MR is small due to following factors: aromatic structure, low mobility, low adsorption and hindrance against electron. Synthesized Fe-p(NIPAM-AA) hybrid microgel is found to be effecient catalyst for reduction of organic pollutants. High percentage reduction is found in nitrophenols among series of substrates due to their small size and less retardation in electron density transfer.

Comparison of reduction time of all substrates

Figure 4 c shows plot of comparison of reduction time of substrates using hybrid microgel as catalyst. Figure 4 c shows the decreasing trend of reduction time as 4-NBA > MB > 4-NP > RB5 > DNP > 3-NP > 4-NAS > CR > MR > CV. Values of reduction time of 4-NBA, MB, 4-NP, RB5, DNP, 3-NP, 4-NAS, CR, MR, and CV are observed 29, 25.5, 23, 13.3, 12.3, 12, 11.6, 9, 7.3, and 5.3 min, respectively. Reduction time of nitroarenes was observed almost lower than that of organic azo dyes. High flux, high adsorption, and more contact time of nitrarenes
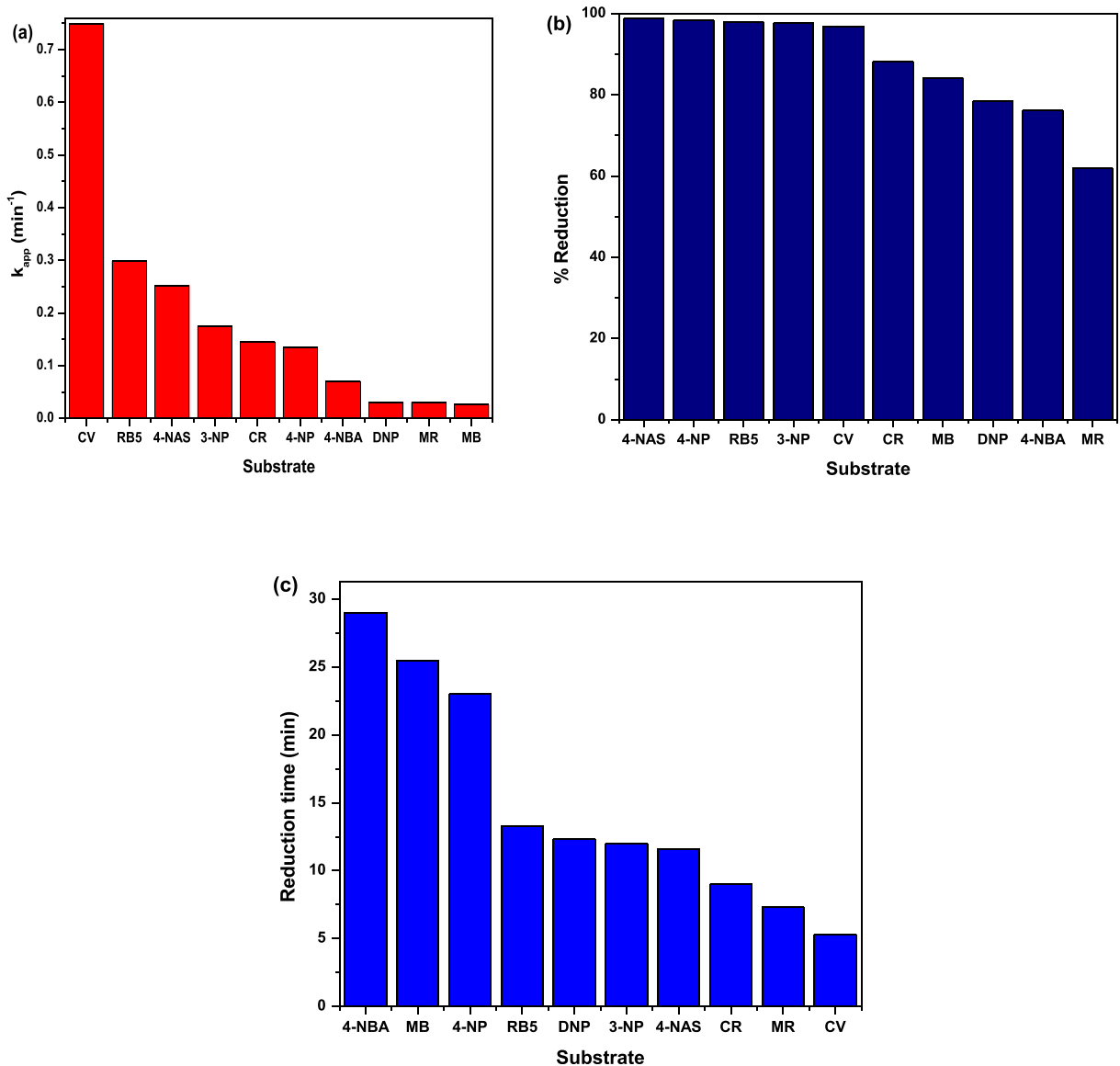
Fig. 4 Parameters calculated after studying catalytic reduction of nitroarenes and azo dyes: **a** k_{app}, **b** percentage reduction, and **c** reduction time

with Fe nanoparticles enhanced the faster reduction of nitroarenes instead azo dyes. Trend shows MB was reduced in short time as compared to other substrates. High flux and adsorption of CV increased its contact time with Fe nanoparticles. Less hindrance of bulky groups is facilitated the rapid reduction of CV. Figure 4 c shows the slowest reduction of 4-NBA as compared with nitroarenes and organic azo dyes. Electrostatic interaction between COO^- of microgel network and 4-NBA may decrease its flux, due to which adsorption and contact time of 4-NBA were also decreased. The reduction time of 4-NP was found smaller than that of MB and 4-NBA due to its easy flux, more contact time, and no hinderance of bulky groups. Reduction time of CV was observed smallest among all substrates. Reduction time of nitroarenes was almost similar to each other. Significant difference in reduction time among various azo dyes was observed (Fig. 4c). Ismail et al. had observed similar reduction time trend as nitrophenols 4-NP $\approx$ 2-NP > CR > MR using Ag nanoparticles supported with tero plant as catalyst (Ismail et al. 2018). So, fast reduction is facilitated by the absence of bulky groups in CV, RB5, and nitrophenols.

Conclusions

Fe nanoparticles were successfully synthsized by in situ reduction within whole microgel network. Size of fabricated Fe nanoparticles lies in 8–40 nm range. Presence of two SPR bands at short and long wavelengths was indicated that Fe nanoparticls of two sizes were synthesized within microgel. Series of nitroarenes and azo dyes were reduced using synthesized Fe-p(NIPAM-AA) hybrid microgel as catalyst. AA facilitates the flux of substrates of different structures and sizes. Siginficant difference in k_{app} values of all substrates is observed. Catalytic activity of hybrid microgel is observed higher for nitroarenes than azo dyes. Complex structure, low flux, and less adsorption of molecules of azo dyes increased its contact time with reducing agent and Fe nanoparticles. Significant reduction in CV and RB5 were observed. k_{app} value of CV is 0.749 min^{-1} which is observed highest among all substrates. Comparison of reduction time and percentage reduction of these substrates were also studied. Maxmium percentage reduction of 4-NP and 4-NAS was observed. Significant reduction in CV was observed in 5.3 min among series of substrates. So, synthsized hybrid microgel is found to be a capable catalyst for reduction of different substrates which possess different structural size and functional group orientation. Newly synthesized product was used for catalytic reduction of series substrates regardless of their chemical structures. Dependence of catalytic activity of catalyst on size, orientation, and hinderance of bulky groups in chemical structres of substatres is also studied.

Compliance with ethical standards

Conflict of interest The authors declare that they have no conflict of interest.

References

Abid HR, Shang J, Ang H-M, Wang S (2013) Amino-functionalized Zr-MOF nanoparticles for adsorption of CO_2 and CH_4. Int J Smart Nano Mater 4:72–82

Bhattacharjee A, Ahmaruzzaman M, Sinha T (2015) A novel approach for the synthesis of SnO_2 nanoparticles and its application as a catalyst in the reduction and photodegradation of organic compounds. Spectrochim Acta Part A Mol Biomol Spec 136:751–760

Bhattacharya S, Eckert F, Boyko V, Pich A (2007) Temperature, pH, and magnetic-field -sensitive hybrid microgels. Small 3: 650–657

Biffis A, Cunial S, Spontoni P, Prati L (2007) Microgel-stabilized gold nanoclusters: powerful "quasi-homogeneous" catalysts for the aerobic oxidation of alcohols in water. J Catal 251:1–6

Calace N, Nardi E, Petronio B, Pietroletti M (2002) Adsorption of phenols by papermill sludges. Environ Pollut 118:315–319

Chang PR, Yu J, Ma X, Anderson DP (2011) Polysaccharides as stabilizers for the synthesis of magnetic nanoparticles. Carbohydr Polym 83:640–644

Chen T, Fang Q, Zhou L, Xu Z, Qiu J, Wang M, Wang J (2019) Comparative study of cross-linked and linear thermo-responsive carriers supported palladium nanoparticles in the reduction of 4-nitrophenol: structure, catalytic activity and responsive catalysis property. React Func Polym 142:104–111

Dong Z, Le X, Li X, Zhang W, Dong C, Ma J (2014) Silver nanoparticles immobilized on fibrous nano-silica as highly efficient and recyclable heterogeneous catalyst for reduction of 4-nitrophenol and 2-nitroaniline. Appl Catal B Environ 158:129–135

Edison TJI, Sethuraman M (2013) Biogenic robust synthesis of silver nanoparticles using Punica granatum peel and its application as a green catalyst for the reduction of an anthropogenic pollutant 4-nitrophenol. Spectrochim Acta Part A Mol Biomol Spec 104:262–264

Eslami S, Ebrahimzadeh MA, Biparva P (2018) Green synthesis of safe zero valent iron nanoparticles by *Myrtus communis* leaf extract as an effective agent for reducing excessive iron in iron-overloaded mice, a thalassemia model. RSC Adv 8: 26144–26155

Farooqi ZH, Khan SR, Hussain T, Begum R, Ejaz K, Majeed S, Ajmal M, Kanwal F, Siddiq M (2014) Effect of crosslinker feed content on catalaytic activity of silver nanoparticles fabricated in multiresponsive microgels. Korean J Chem Eng 31:1674–1680

Farooqi ZH, Naseem K, Begum R, Ijaz A (2015a) Catalytic reduction of 2-nitroaniline in aqueous medium using silver nanoparticles functionalized polymer microgels. J Inorg Organomet Polym Mater 25:1554–1568

Farooqi ZH, Sakhawat T, Khan SR, Kanwal F, Usman M, Begum R (2015b) Synthesis, characterization and fabrication of copper nanoparticles in N-isopropylacrylamide based copolymer microgels for degradation of p-nitrophenol. Mater Sci Poland 33:185–192

Fu Y, Xu P, Huang D, Zeng G, Lai C, Qin L, Li B, He J, Yi H, Cheng M (2019) Au nanoparticles decorated on activated coke via a facile preparation for efficient catalytic reduction of nitrophenols and azo dyes. Appl Surf Sci 473:578–588

Ghosh BK, Hazra S, Naik B, Ghosh NN (2015) Preparation of Cu nanoparticle loaded SBA-15 and their excellent catalytic activity in reduction of variety of dyes. Powder Technol 269:371–378

Huang X, El-Sayed MA (2010) Gold nanoparticles: optical properties and implementations in cancer diagnosis and photothermal therapy. J Adv Res 1:13–28

Hudson R, Ishikawa S, Li CJ, Moores A (2013) Magnetically recoverable $CuFe_2O_4$ nanoparticles as highly active catalysts

for $C_{sp}{}^3$–C_{sp} and $C_{sp}{}^3$–$C_{sp}{}^3$ oxidative cross-dehydrogenative coupling. Syn Lett 24:1637–1642

Ismail M, Khan M, Khan SB, Akhtar K, Khan MA, Asiri AM (2018) Catalytic reduction of picric acid, nitrophenols and organic azo dyes via green synthesized plant supported Ag nanoparticles. J Mol Liq 268:87–101

Karg M, Pastoriza-Santos I, Rodriguez-Gonzalez B, von Klitzing R, Wellert S, Hellweg T (2008) Temperature, pH, and ionic strength induced changes of the swelling behavior of PNIPAM– poly (allylacetic acid) copolymer microgels. Langmuir 24:6300–6306

Khan SR, Farooqi ZH, Waheed uz Z, Ali A, Begum R, Kanwal F, Siddiq M (2016) Kinetics and mechanism of reduction of nitrobenzene catalyzed by silver-poly(N-isopropylacrylamide-co-allylacetic acid) hybrid microgels. Mater Chem Phys 171:318–327

Liu YY, Liu XY, Yang JM, Lin DL, Chen X, Zha LS (2012) Investigation of Ag nanoparticles loading temperature responsive hybrid microgels and their temperature controlled catalytic activity. Colloid Surf A 393:105–110

Martinez-Huitle CA, Ferro S (2006) Electrochemical oxidation of organic pollutants for the wastewater treatment: direct and indirect processes. Chem Soc Rev 35:1324–1340

Naseem K, Begum R, Farooqi ZH (2018) Platinum nanoparticles fabricated multiresponsive microgel composites: synthesis, characterization, and applications. Polym Compos 39:2167–2180

Ott WR, Roberts JW (1998) Everyday exposure to toxic pollutants. Sci Am 278:86–91

Pawar RC, Khare V, Lee CS (2014) Hybrid photocatalysts using graphitic carbon nitride/cadmium sulfide/reduced graphene oxide (gC_3N_4/CdS/RGO) for superior photodegradation of organic pollutants under UV and visible light. Dalton Trans 43:12514–12527

Pich A, Karak A, Lu Y, Ghosh AK, Adler HJP (2006a) Tuneable catalytic properties of hybrid microgels containing gold nanoparticles. J Nanosci Nanotechnol 6:3763–3769

Pich A, Karak A, Lu Y, Ghosh AK, Adler HJP (2006b) Preparation of hybrid microgels functionalized by silver nanoparticles. Macromol Rapid Commun 27:344–350

Pouretedal H, Sabzevari S (2011) Photodegradation study of Congo red, methyl orange, methyl red and methylene blue under simulated solar irradiation catalyzed by ZnS/CdS nanocomposite. Desalin Water Treat 28:247–254

Sarkar S, Banerjee A, Halder U, Biswas R, Bandopadhyay R (2017) Degradation of synthetic azo dyes of textile industry: a sustainable approach using microbial enzymes. Water Cons Sci Eng 2:121–131

Shah LA, Haleem A, Sayed M, Siddiq M (2016) Synthesis of sensitive hybrid polymer microgels for catalytic reduction of organic pollutants. J Environ Chem Eng 4:3492–3497

Shahid M, Farooqi ZH, Begum R, Arif M, Wu W, Irfan A (2019) Hybrid microgels for catalytic and photocatalytic removal of nitroarenes and organic dyes from aqueous medium: a review. Crit Rev Anal Chem:1–25. https://doi.org/10.1080/10408347.2019.1663148

Shi X, Wang SH, Swanson SD, Ge S, Cao Z, Van Antwerp ME, Landmark KJ, Baker JR Jr (2008) Dendrimer-functionalized shell-crosslinked iron oxide nanoparticles for in-vivo magnetic resonance imaging of tumors. Adv Mater 20:1671–1678

Soğukömeroğulları HG, Karataş Y, Celebi M, Gülcan M, Sönmez M, Zahmakiran M (2019) Palladium nanoparticles decorated on amine functionalized graphene nanosheets as excellent nanocatalyst for the hydrogenation of nitrophenols to aminophenol counterparts. J Hazard Mater 369:96–107

Ulbrich K, Hola K, Subr V, Bakandritsos A, Tucek J, Zboril R (2016) Targeted drug delivery with polymers and magnetic nanoparticles: covalent and noncovalent approaches, release control, and clinical studies. Chem Rev 116:5338–5431

Veerakumar P, Chen SM, Madhu R, Veeramani V, Hung CT, Liu SB (2015) Nickel nanoparticle-decorated porous carbons for highly active catalytic reduction of organic dyes and sensitive detection of Hg (II) ions. ACS Appl Mater Interf 7:24810–24821

Velayudhan Nair Girija V, Vasu S (2019) Synthesis and characterization of iron oxide nanoparticles by thermal decomposition method of iron (III) chelates. Int J Nanosci Nanotechnol 15:65–73

Wang J, Chen B (2015) Adsorption and coadsorption of organic pollutants and a heavy metal by graphene oxide and reduced graphene materials. Chem Eng J 281:379–388

Wu W, Shen J, Li Y, Zhu H, Banerjee P, Zhou S (2012) Specific glucose-to-SPR signal transduction at physiological pH by molecularly imprinted responsive hybrid microgels. Biomaterials 33:7115–7125

Wunder S, Lu Y, Albrecht M, Ballauff M (2011) Catalytic activity of faceted gold nanoparticles studied by a model reaction: evidence for substrate-induced surface restructuring. ACS Catal 1:908–916

Yamjala K, Nainar MS, Ramisetti NR (2016) Methods for the analysis of azo dyes employed in food industry–a review. Food Chem 192:813–824

Yoo SI, Kwon JH, Sohn BH (2007) Single layers of diblock copolymer micelles for the fabrication of arrays of nanoparticles. J Mater Chem 17:2969–2975

Zhang Y, Zhang J, Cheng Z, Xu J (2011) Morphology dependence effect of CuO nanostructures on their Cl_2 sensing properties. Sens Lett 9:175–178